

Introduction

Advances in MR microimaging technology have made possible image-based analysis of the three-dimensional microstructure of connective tissues on a resolution scale of 100μm or better. Of particular relevance are cancellous bone (1, 2) and articular cartilage (3, 4). In vivo, one of the potential obstacles to achieve adequate resolution is physiologic and subject motion. Here we evaluate the effectiveness of the navigator motion correction method (NAV) in subjects who underwent microimaging of the ultradistal forearm, and compare it with the autofocusing technique (AF) for 2D translational motion correction. Criteria for assessment of efficacy of the algorithms are (a) visual inspection of the images, (b) the incremental changes in the derived structural parameters, and (c) changes in image entropy.

Materials and Methods

Forty-nine subjects were imaged on a GE Signa 1.5T Epic 5.6 MR system equipped with Echospeed gradients. A 3D FLASE pulse sequence (5) was used to obtain high-resolution images of the right distal radius with a resolution of 137x137x350μm³ in 11 min scan time (512x256x32 matrix size). FLASE, a spin-echo sequence optimized for short-TR imaging by using a large flip angle (>90°) excitation pulse, was fitted with navigator readout gradients immediately following the standard image readout and rewinding of the gradients. The navigator readouts are alternated between the two in-plane axes to detect motion in both directions (6).

In-plane motion was determined from image projections using the least-squares method (7), and images with and without navigator correction reconstructed. In addition, autofocusing based on minimizing image entropy (8) was applied to one slice in each uncorrected image set of 10 subjects whose bone volume fraction (BVF) (9) change after NAV correction was above an arbitrary threshold of 0.007. The AF correction was then applied to all slices of each subject (since slice-encoding is cycled contiguously at each phase-encoding step, the same motion information can be used for all slices). Image sharpening via AF was processed with 2 iterations: first using larger groups of views and next with fewer views per set. In each case, the number was also increased with increasing distance from the k-space center, since the signal is lower in those regions and thus is more prone to errors in motion approximation. Following motion correction, entropy and BVF were calculated for comparison.

Results and Conclusions

Figure 1 shows a histogram of changes in calculated BVF before and after NAV correction was applied, showing significant changes in the parameter obtained with motion compensation. Increases in the apparent BVF after motion compensation are consistent with previously reported observations showing that motion underestimates BVF (6).

Table 1 compares the changes in entropy (E) and BVF after motion correction with AF and NAV techniques. Although not as effective as the NAV method, the AF technique was found to significantly improve image sharpness, resulting in reduced entropy and increased BVF. The images in Fig. 3 from one of the subjects show improved detail and reduced blurring with both motion correction techniques.

Although the NAV technique is more effective, AF is advantageous in that there is no need to collect additional data, which can become quite large in high-resolution, multiple slice imaging studies. One of the limiting factors of the AF method, how-

ever, may be its long processing times, further exacerbated with increasing number of iterations. Also, whereas with NAV it is possible to correct for motion at every slice- or phase-encoding view, AF correction is based on reconstructed images, limiting the time resolution of motion approximation in 3D imaging to the number of slices times TR.

Conclusion

This work demonstrates that both 2D navigator and autofocusing techniques are effective in reducing motional blurring in high-resolution in vivo images. For the application studied, the navigator technique performed somewhat better, as confirmed by lower image entropy and higher BVF, as well as assessed visually.

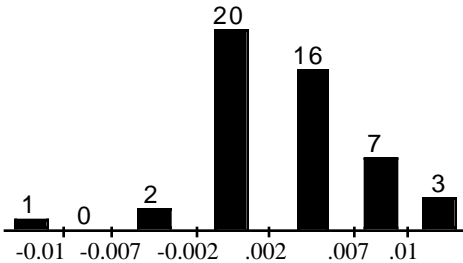
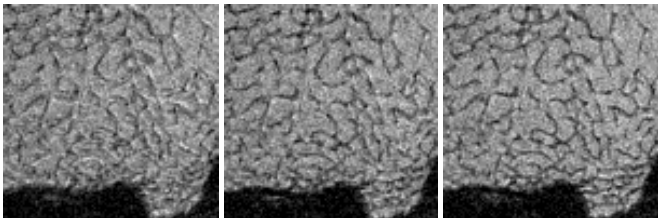


Fig. 1 Histogram of ΔBVF (BVF_{post} - BVF_{pre}).

Table 1 Entropy (E) and BVF changes for the two methods.

Subject	ΔE % (AF)	ΔE % (NAV)	ΔBVF % (AF)	ΔBVF % (NAV)	BVF (Uncorr)
1	-0.47	-0.90	3.1	4.9	0.146
2	-0.21	-0.37	4.3	6.6	0.129
3	-0.57	-0.85	8.9	8.0	0.106
4	-0.15	-0.25	5.0	7.8	0.100
5	-0.19	-0.75	2.3	8.0	0.116
6	-0.51	-0.64	10.1	8.7	0.109
7	-0.23	-0.70	4.5	8.9	0.165
8	-0.39	-0.57	4.1	7.0	0.159
9	-0.16	-0.53	2.7	5.1	0.143
10	-1.31	-1.61	7.0	7.9	0.157
Avg	-0.42	-0.72	5.2	7.3	



a) No correction b) AF corrected c) NAV corrected
Fig. 2 Comparison of images before (a) and after correction via autofocusing (b) and navigator echoes.

References

1. C. L. Gordon, et al, *Med. Phys.* **24**, 585 (1997).
2. F. W. Wehrli, et al, *Radiology* **206**, 347 (1998).
3. W. Gründer, et al, *Proc. ISMRM*, vol. 1, p. 405.
4. G. E. Gold, et al, *Proc. ISMRM*, vol. 1, p. 43.
5. J. Ma, et al, *Magn Reson Med* **35**, 903 (1996).
6. H. K. Song, et al, *Proc. ISMRM*, vol. 3, p. 2109.
7. Y. Wang, et al, *Magn Reson Med* **36**, 117 (1996).
8. D. Atkinson, et al, *IEEE Trans. Med. Imag.* **16**, 903 (1997).
9. S. N. Hwang, et al, *Med. Phys.* **24**, 1255 (1997).